Centrality dependence of the parton bubble model for high-energy heavy-ion collisions and fireball surface substructure at energies available at the BNL relativistic heavy ion collider (RHIC)

S. J. Lindenbaum
City College of New York, New York city, New York 10031, USA and
Brookhaven National Laboratory, Upton, New York 11973, USA

R. S. Longacre
Brookhaven National Laboratory, Upton, New York 11973, USA

(Received 25 June 2008; revised manuscript received 21 September 2008; published 10 November 2008)

In an earlier paper we developed a QCD-inspired theoretical parton bubble model (PBM) for RHIC/LHC. The motivation for the PBM was to develop a model that would reasonably quantitatively agree with the strong charged particle pair correlations observed by the STAR Collaboration at RHIC in Au + Au central collisions at $\sqrt{s_{NN}} = 200$ GeV in the transverse momentum range 0.8 to 2.0 GeV/c. The model was constructed to also agree with the Hanbury Brown and Twiss (HBT) observed small final-state source size ∼2 fm radii in the transverse momentum range above 0.8 GeV/c. The model assumed a substructure of a ring of localized adjoining ∼2 fm radius bubbles perpendicular to the collider beam direction, centered on the beam, at midrapidity. The bubble ring was assumed to be located on the expanding fireball surface of the Au + Au collision. These bubbles consist almost entirely of gluons and form gluonic hot spots on the fireball surface. We achieved a reasonable quantitative agreement with the results of both the physically significant charge-independent (CI) and charge-dependent (CD) correlations that were observed. In this paper we extend the model to include the changing development of bubbles with centrality from the most central region where bubbles are very important to the most peripheral where the bubbles are gone. Energy density is found to be related to bubble formation and as centrality decreases the maximum energy density and bubbles shift from symmetry around the beam axis to the reaction plane region, causing a strong correlation of bubble formation with elliptic flow. We find reasonably quantitative agreement (within a few percent of the total correlations) with a new precision RHIC experiment that extended the centrality region investigated to the range 0%–80% (most central to most peripheral). The characteristics and behavior of the bubbles imply they represent a significant substructure formed on the surface of the fireball at kinetic freezeout.

DOI: 10.1103/PhysRevC.78.054904 PACS number(s): 25.75.Gz, 12.38.Mh

I. INTRODUCTION AND REVIEW OF MODEL

In the mid 1980s L. van Hove [1] proposed a bubble model as a way of finding convincing evidence for a quark-gluon plasma (QGP). His model based on a string calculation predicted that one to perhaps a few observable localized rapidity bumps would appear in the final state of some events and he gave a prescription for experimentally finding them. We searched for these in all relevant data, but we nor anyone else ever found experimental evidence for the rapidity bumps.

There were numerous other bubble models and some charge correlation models proposed. Some examples of these are in Refs. [2–7]. However, to our knowledge no significant experimental evidence has been found for any of these.

In a previous publication [8] we proposed a parton bubble model (PBM) for central (impact parameter near zero) high-energy heavy-ion collisions at RHIC/LHC that contains a substructure consisting of an 8-fm-radius single ring of a dozen adjoining 2-fm-radius bubbles transverse to the collider beam direction, centered on the beam, and located at or near midrapidity on the expanding surface of the fireball at kinetic freezeout. The bubble radius and the bubble ring radius were estimated by considering the Hanbury-Brown and Twiss (HBT [9]) observations and other general considerations utilizing the blast wave model. We assumed these bubbles (gluonic hot spots) are likely the final-state result of QGP formation. Thus this is the geometry for the final-state kinetic freezeout of the QGP bubbles on the surface of the expanding fireball treated in a blast wave model. In the central (near impact parameter 0) midrapidity region at RHIC we are observing the region where the highest energy densities and temperatures (parton energies) are produced. The experimentally observed $\sqrt{s_{NN}} = 200$ GeV central Au + Au collisions at RHIC [10] produce initial energy densities [11] that exceed those predicted by lattice quantum chromodynamics (QCD) as sufficient for production of a QGP [12].

This single bubble ring resides at midrapidity on the surface of the expanding fireball at kinetic freezeout. Thus each bubble would emit a considerable fraction of final-state particles (observed experimentally) resulting from the QGP state. The fraction of all the final-state particles from bubbles is ∼1/2. There would be very little reinteraction for particles emitted outward from the surface because the final-state surface of the fireball is at kinetic freezeout. The bubble substructure (surrounded by cooler background) results in the lumpy surface of the fireball at kinetic freezeout. Section II presents more detail on the assumptions made, the development, and construction of the PBM.

The PBM successfully explained in a reasonably quantitative manner all of the particle pair correlations in a precision

STAR central production experiment [10]. See Sec. 4 of Ref. [8] for this comparison. In Ref. [8] some aspects of quark-quark recombination were compared with the PBM and a good agreement was obtained (see Sec. 5 of Ref. [8]).

In this paper we extend the model of Ref. [8] to consider the case of varying the centrality bins (Sec. III). We wish to compare with a new RHIC $\sqrt{s_{NN}} = 200$ GeV minimum bias Au + Au analysis that covered the 0%–80% centrality range [13].

This paper is organized as follows: Section I gives an introduction. Section II summarizes the assumptions made in the prior model (PBM) for the central region (0%–10% centrality [8]) Section II also discusses the relevance and the reasoning behind these assumptions. Section III discusses extending the PBM so that it becomes able to reasonably quantitatively fit and explain the new 0%–80% centrality high-precision data [13]. Section IV discusses general characteristics of the PBM. Section V presents and discusses a comparison of the experimentally determined charge-independent correlation with the extended version of the PBM (PBME) as a function of percent centrality. Section VI presents and discusses a comparison of the experimentally determined charge-dependent correlation with the PBME as a function of percent centrality. Section VII presents further details of the PBME bubble correlation. Section VIII gives the summary and discussion.

II. ASSUMPTIONS AND DEVELOPMENT OF THE PBM

Our goal for the past two decades was to develop a model of bubble production in relativistic heavy-ion collisions assumed to originate from a QGP, which could be reasonably quantitatively compared with relevant experimental data of sufficient precision and scope. Thus hopefully we could obtain convincing, or at least substantial, evidence for the existence of bubble production. Since this is a process that clearly involves strong nonperturbation QCD, pQCD calculations can serve only as a rough guide.

Thus we concluded we needed to obtain a strong hint from experimental data as evidence for possible bubble substructure to proceed to build a realistic model. The failures of obtaining significant experimental evidence for the many bubble models that did not incorporate such a strong hint from the experimental data led us to conclude that it was essential to obtain one from experimental observations. Then one could build the bubble model based on observations to provide a quantitative description of the data.

We utilize a two-particle correlation function in the two-dimensional (2-D) space of $\Delta\phi$ versus $\Delta\eta$. The azimuthal angle ϕ of a particle is defined by the angle of the particle with respect to the vertical axis that is perpendicular to the beam axis and is measured in a clockwise direction about the beam. The angle $\Delta\phi$ is the difference, $\phi_1 - \phi_2$, of the ϕ angle of a pair of particles (1 and 2). The pseudorapidity η of a particle is measured along one of the beam directions and $\Delta\eta$ is the difference, $\eta_1 - \eta_2$, of the η values of a pair of particles (1 and 2).

The 2-D total correlation function is defined as

$$C(\Delta\phi, \Delta\eta) = S(\Delta\phi, \Delta\eta)/M(\Delta\phi, \Delta\eta), \quad (1)$$

where $S(\Delta\phi, \Delta\eta)$ is the number of pairs at the corresponding values of $\Delta\phi$, $\Delta\eta$ coming from the same event, after we have summed over all the events, and $M(\Delta\phi, \Delta\eta)$ is the number of pairs at the corresponding values of $\Delta\phi$, $\Delta\eta$ coming from the mixed events, after we have summed over all our created mixed events. A mixed event pair has each of the two particles chosen from a different event. We make on the order of ten times the number of mixed events as real events. We rescale the number of pairs in the mixed events to be equal to the number of pairs in the real events.

The behavior of the HBT quantum interference radii [9], especially R_s, was interpreted as indicative of observation of spatial radii ∼2 fm in RHIC central Au + Au collisions at $\sqrt{s_{NN}} = 200$ GeV for $p_t > 0.8$ GeV/c. R_s reduced from ∼6 to ∼2 fm as p_t increased from ∼0.2 GeV/c to greater than ∼0.8 GeV/c. HBT quantum interference is by necessity only measured for pairs of charged particles of the same sign with small difference in momentum. In our model all particles coming from a bubble are constrained to come from a ∼2-fm radius. Particles above 0.8 GeV/c p_t that come from different bubbles differ in momentum such that they do not show HBT quantum interference.

The generally accepted explanation for observing these increasingly smaller final-state HBT radii as p_t increased was that radial flow increasingly focused the viewed region of the overall final-state source into a smaller volume as p_t increased. We refer to this phenomenon as phase-space focusing due to flow. We realized (in our first bubble model paper [14] published in 2003) that flow phase-space focusing implies that the viewed region on the surface for $p_t > 0.8$ GeV/c of the fireball would have a volume with radius of ∼2 fm. Within this volume a hot source producing a larger number of particles would move out away from the surface, and being focused together would lead to an increase of particles emitted in an angular region. However, the HBT correlation function has the property that a ring of essentially similar bubbles as assumed in our PBM would image on top of each other, forming an average bubble that HBT would be viewing. The lower p_t cut of 0.8 GeV/c would allow HBT to view and resolve this average bubble formed from differences in momentum of two particles for p_t above 0.8 GeV/c. Our model populated these HBT viewed regions with a ring of bubbles or gluonic hot spots, producing a larger number of particles with an angular correlation. We form a correlation function based on the difference of angles between two charged particles that images the 12 bubbles on top of each other.

It is important to note that we have calculated that the correlations observed at RHIC are strong enough so that if there was only one bubble instead of a ring of bubbles distributed around the azimuth as our PBM assumed, one would produce an angular region with huge amplitude spikes in individual events. These spikes are not observed in individual events at RHIC. Therefore the RHIC correlation data have to be built of smaller distributed correlated regions as assumed by the PBM.

We had used a virtually identical bubble ring and the same correlation function in our first bubble model [14], which was able to predict and subsequently explain important general characteristics of the experimental analysis of the two-charged-particle correlation data for central collisions [10].

This experimental paper used the p_t cuts developed in our 2003 paper, $0.8 < p_t < 2.0$ GeV/c. The 2 GeV/c cut was employed to make jet contamination negligible. The angular correlations used the differences of the azimuthal angles ($\Delta\phi$) and the differences of psuedorapidity ($\Delta\eta$) of all charge particle pairs that had the property that imaged all bubbles in the ring on top of each other. This allowed the phase-space focusing by radial flow to provide consistency with the observed correlation data analyses and the HBT observations.

An important assumption made in our PBM is that in a central heavy-ion collision (e.g., Au + Au) at high RHIC energies a high density of energetic partons (virtually all gluons) form a dense opaque fireball. This dense opaque fireball has a large amount of radial flow and can be described very well by a blast wave model. The usually employed blast wave model we used [9] has its maximum velocity at the surface of the fireball at kinetic freezeout of approximately $(3/4)c$.

In a theoretical pQCD calculation [15] in 1987 it was concluded that jets formed with initial parton transverse momenta of around 3 GeV/c (also applicable down to 2 GeV/c) would become thermalized in a $\sqrt{s_{NN}} = 200$ GeV U + U collision at RHIC and would not escape from the system. Therefore these jets would not result in the correlations observed at RHIC [10]. One could speculate that these thermalized jets form the dense opaque fireball.

There is direct experimental evidence of strong quenching of high-p_t particles at RHIC (e.g., Refs. [16–18]). An experimental result that is independent of our model demonstrates that in the central region charged particles with p_t in the range $0.8 < p_t < 4.0$ GeV/c are emitted from the surface of the dense opaque fireball. This point was demonstrated in Sec. IV B of Ref. [13]. We quote the last three sentences from this Sec. IV B: "This surface or near surface hadronization and emission from the fireball both occur in the central region and all other centralities where there is appreciable particle density. In the most peripheral bins the particle density is low enough to allow undisturbed fragmentation and thus no change in the CD correlation. Thus the CD behavior is consistent with a surface emission model such as Ref. [8]." This result implies that surface or near-surface emission occurs for charged particles with $0.8 < p_t < 4.0$ GeV/c for all centralities.

The HIJING event generator [19] combines PYTHIA jets [20] and the Lund model [21] and thus was a familiar base for constructing our PBM. As we had done in our earlier bubble model [14], we replaced the PYTHIA jets in HIJING with our bubble ring. Momentum, energy, and charge conservation are all satisfied within the bubble ring in the PBM. The bubble ring becomes the source of emitted particle correlation generated by PYTHIA, which we used for fragmentation of the bubbles. We made the approximation that hard jet particles are essentially removed or have their correlations removed by quenching. The only remaining particles from HIJING are the beam-jet fragmentation particles, which are soft and have no correlation. These particles become our background particles in the PBM. However, we did include the effects of elliptic flow [22] on the soft beam-jet fragmentation particles, since elliptic flow does generate a small $\cos(2\Delta\phi)$ term in the correlation even in the central collisions. The procedure we employed was to, in each event, determine the reaction plane and modulate the soft beam fragmentation particles by the elliptic flow term $2v_2\cos(2\Delta\phi)$, which was a sufficient approximation for elliptic flow effects. Thus the elliptic flow effects were put into the model on an event-by-event basis. In the PBM we used angular correlations of charge particle pairs to predict and fit the experimentally determined correlations [10].

In Fig. 3 of the PBM publication [8] we schematically show a number (3–4) of parallel parton showers contained in each bubble. The parton showers must be parallel to give results that are consistent with the experimental analysis of angular correlations.

The particle production from our bubbles uses a similar parton QCD shower fragmentation as a jet with a well-defined ϕ angle (Fig. 2 of the PBM [8]). The p_t distribution of the partons inside the bubble is similar to that in pQCD but has a suppression in the high-p_t region like the data [16–18]. The 3–4 partons have different longitudinal momentum. At kinetic freezeout we used PYTHIA fragmentation functions [20] for the bubble fragmentation to form the final-state emitted charged particles.

Models that successfully predict and fit nonperturbative QCD experimental results reasonably almost always have to have some parameters adjusted when comparing with experimental data. In the PBM there are two such adjustable parameters: the number of partons in a bubble and the longitudinal momenta of the partons. Ever since Landau discovered in cosmic rays that excited nuclear fireballs exhibited a longitudinal expansion this fact was well known. Adjusting the longitudinal momenta of the partons is obviously necessary to explain the expansion in $\Delta\eta$ in the central production experiment [10]. The two parameters in the PBM were adjusted for a set number of bubbles by comparing the PBM fit to the experimentally determined final-state charge pair correlation.

In our models (e.g., PBM) the experimental correlation data analysis we are comparing to utilizes the correlations of charge particle pairs. There are two types of such correlated pairs, namely unlike-sign charge pairs (US) and like-sign charge pairs (LS). The total sample of correlated charge pairs generated and emitted in the final state of a theoretical model is equal to the average of the US and LS correlations [(US + LS)/2]. In an experiment the total sample detected depends on the acceptance and efficiency of the detector. One makes cuts on the theoretical model to account for these effects. However, the correlation function used in Eq. (1) is conventionally used in experimental analyses and is drastically independent of acceptance effects as stated in Sec. 2.1 [8], allowing reasonable comparisons.

The charge-independent (CI) correlation is conventionally defined as the unlike-sign charge pairs correlation plus the like-sign charge pairs correlation. The total correlation derived when using all particle pairs independent of what charge signs are used to form the correlation is equal to CI/2. Thus CI/2 gives the average structure of the correlated emitting sources independent of charge and represents the overall physical phenomenon.

The charge-dependent (CD) correlation is conventionally defined as US − LS. The subtraction of the total like-sign charge pairs correlation in forming the CD is equivalent to

removal of the opposite-sign charge pairs that are not from the same space-time region where charge has to balance [10, 23]. Therefore the CD is expected to represent the correlation of unlike-sign pairs from the same space-time region where charge is balanced as modified by interaction with the medium. In our surface emission model (PBM) the interaction with the medium is absent; therefore, the CD is expected to exhibit the correlation of PYTHIA jets that are produced in vacuum.

In Sec. 4.2 of Ref. [8] we compare the total CI correlations of PBM and precision experimental correlation data [10]. We adjusted the two parameters by comparing the CI of the PBM with the CI of the data. We show that the PBM and the data agree within less than 10% of the total CI correlation, which is a reasonably quantitative agreement.

In Sec. 4.3 of Ref. [8] we compare the CD correlations of PBM with the experiment by making use of the fact that the net charge fluctuation suppression is directly related to an integral over the CD. Thus we compared the net charge fluctuation suppressions of the data with the PBM and found agreement within errors. We did the comparison of the CD in this way since the authors of the experimental paper with which we compared the model considered this to be an important aspect of the CD correlation and chose to treat the CD in this manner.

III. EXTENSION OF PBM TO COVER 0%–80% CENTRALITIES

The PBM is a successful bubble model for central heavy-ion (e.g., Au + Au) collisions at the highest energy at RHIC, as discussed in the previous section. However, an interesting question that arises is what would happen to bubble production and the general characteristics of charge pair correlations as centrality varies from most central (impact parameter near zero) to peripheral collisions. The PBM has been successfully tested in the centrality range of approximately 0%–10%. A new precision RHIC minimum-bias trigger data analysis for Au + Au collisions at $\sqrt{s_{NN}} = 200$ GeV in the transverse momentum range from 0.8 to 4.0 GeV/c covers the 0%–80% centrality range [13] and is ideally suited for investigating the varying centrality evolution of the PBM. This experimental analysis was done in a manner that was a logical extension of the central production paper [10]. The data, the charge particle pairs correlations (US and LS), and the CI and the CD were treated in a similar manner but analyzed and fit separately in each of nine centrality bins.

In the data analysis [13] the most central US, LS, and CI bins were consistent with the results of the prior central production experiment. However, as one moves from central to peripheral bins a jetlike component is increasingly evident (in the data analysis) till the most peripheral bins where there are only jetlike correlations. The elliptic flow amplitude $2v_2^2$ as part of the correlation increases as one moves to more peripheral centralities. This flow reaches its maximum at 40%–50% centrality (see Fig. 28 of Ref. [13]).

We will proceed to extend the PBM to include the entire 0%–80% centrality region. We name this extended version of the PBM the PBME. Several obvious characteristics of the experimental and theoretical analysis that must be included in this extension of the model to PBME are discussed in the following.

The previous central collision bubble ring geometry was well suited for the most central collisions situation since the highest energy densities are circular around the beam, which is the expected geometric symmetry. As one moves from central toward peripheral the decreasing size and change of shape of the overlap region of the two Au nuclei determines where the energy densities are highest. The overlap of matter in the two Au nuclei becomes greater in the reaction plane region, whereas the overlap of matter becomes less outside of the reaction plane. This breaking of symmetry will modify the overall spatial shape and location of the bubbles.

The effects of elliptic flow [22] on the events in each centrality bin were put into the model by using the same procedure we used as previously described in Sec. II for the PBM. The procedure we employed was to, in each event, determine the reaction plane and modulate the soft beam fragmentation particles by the elliptic flow term $2v_2\cos(2\Delta\phi)$, which was a sufficient approximation for elliptic flow effects. Thus the elliptic flow effects were put into the model on an event-by-event basis.

Jet quenching is largest in the most central collisions and decreases as one moves to more peripheral bins. We found a sufficient way to put the effects of strong jet quenching in the central collisions. We set jet quenching to its maximum in HIJING for 0%–30% centralities by removing all jets (i.e., they are quenched away). For centralities 30%–80% we use the non-jet-quenching version of HIJING and thus all jets become part of the event. The soft beam jet particles have elliptic flow as previously described.

We relied on the blast wave to determine the geometry of where the energy density is highest. These regions of high energy density are where bubbles are formed. In the final state at kinetic freezeout the bubbles are located on the fireball (blast wave) surface, which is the source of emitted correlated charge particle pairs generated by PYTHIA fragmentation of the bubbles. Thus the blast wave determined the location, number, and geometry of the bubbles.

IV. GENERAL CHARACTERISTICS OF THE PBME

For the most central bin we have the same bubble geometry and partons per bubble as in Ref. [8], namely 12 bubbles and 3–4 partons per bubble. As we move away from the most central bin the number of partons per bubble decreases, dropping to 3, then 2, and finally to 1 at 50%–60% centrality. The number of bubbles formed per event decreases from 12 in the most central bin to 0.3 in the 50%–60% bin (see Table I).

The most central collisions have a bubble ring symmetry about the beam axis (see Fig. 1 of Ref. [8]). The region of highest energy density will also be symmetric about this axis and the ring of bubbles is the expected geometry. As we move to more peripheral collisions the symmetry becomes defined by the reaction plane. The region of highest energy density becomes more concentrated in the region of the reaction plane. Therefore it is reasonable to expect the ring symmetry will be broken and the bubbles farthest from the reaction plane would disappear. Comparing 0%–5% centrality to 5%–10%

TABLE I. Parameters of bubble model with centrality.

Centrality	Bubbles per event	Partons per bubble
0%–5%	12	3–4
5%–10%	10	3
10%–20%	7	3
20%–30%	5	3
30%–40%	1.5	2
40%–50%	0.6	2
50%–60%	0.3	1

centrality we find that the 12 bubbles reduce to 10 bubbles with the bubbles perpendicular to the reaction plane no longer present. For 10%–20% the number drops to 7 bubbles with 4 bubbles being near the reaction plane and 3 appearing above and below the plane, whereas for 20%–30% we drop to 5 bubbles with 4 bubbles being near the reaction plane and only 1 appearing above or below the plane. Moving to 30%–40%, 40%–50%, and 50%–60% we find that the bubbles are in the reaction plane region with the probability per event of making a bubble being 1.5, 0.6, and 0.3, respectively (see Table I). These changes in bubble production are due to the decrease in energy density as the percent centrality range becomes more peripheral, which decreases the overlap region of the Au + Au colliding nuclei.

The STAR experiment has measured charged particle pairs correlations for minimum-bias Au + Au events at $\sqrt{s_{NN}} =$ 200 GeV [13]. The p_t range of these data is 0.8 to 4.0 GeV/c for the entire 0°–360° ϕ range and an η range of $|\eta| < 1.0$. Both the experimental data analysis compared to and the PMBE model utilize 2-D $\Delta\phi$ $\Delta\eta$ correlations. See examples of these 2-D perspective plots in Refs. [8,10] and Figs. 11–12 (this paper).

To compare and present these 2-D plots for the new data [13] and the PBME we divided the entire $\Delta\eta$ region into five $\Delta\eta$ bins, which covered the entire $\Delta\eta$ range. Each $\Delta\eta$ bin could then be presented as a one-dimensional projection and a comparison between data and model can be made. The five $\Delta\eta$ bins were 0.0 to 0.3, 0.3 to 0.6, 0.6 to 0.9, 0.9 to 1.2, and 1.2 to 1.5. In each of these five $\Delta\eta$ bins the $\Delta\phi$ correlations for the charged particles covered the entire $\Delta\phi$ range from 0° to 180°. Because of the demonstrated symmetry in the data and the model the 360° $\Delta\phi$ range that was experimentally detected was folded, resulting in the 180° ranges.

V. CHARGE-INDEPENDENT CORRELATION

In this section we compare the PBME-predicted CI correlations with the STAR experimental analysis results [13]. The two-particle correlations are formed from two different types of charge particle pairs:

(i) unlike-sign charge pairs and
(ii) like-sign charge pairs.

The CI total correlation then equals the sum (US + LS), which is the sum of the CI signal plus background correlations in the final state after kinetic freezeout. Thus it is twice the average of the total two-particle correlation observed in the detector (STAR Time Projection Chamber; TPC). The entire CI correlation (signal plus background) is used for comparing the analysis results with the model. This eliminates any model dependence on the separation of signal from background. Certain necessary corrections and cuts in the experimental analysis were applied to the PBME (this paper) so that a quantitative comparison could be made with the experimental analysis. The CI displays the average correlation structure of the emitting sources in the final state after kinetic freezeout and thus is physically significant.

The five plots comparing the experimental analysis of the CI and the PBME fits are shown in Figs. 1–5. On the vertical axis the CI is multiplied by the average event multiplicity within the particular centrality bin shown by the symbols on the plot. This procedure is necessary when one compares different centralities to make the comparison independent of multiplicity.

The correlation function is given in Eq. (1). The experimentally observed correlation has a numerator that is proportional to the number of correlated particle pairs, which itself is proportional to the multiplicity. However, the denominator is proportional to the total number of pairs that can be formed, which is proportional to the square of the multiplicity. Therefore to make comparisons of different centralities or other experiments one multiplies by the average multiplicity to remove the dependence on the multiplicity. This procedure is referred to as multiplicity scaling or multiplicity scaled.

For each centrality we generated 500,000 simulated events with the bubble geometries just presented. The impact parameter range of HIJING for the different centralities is given in Table II. See Table I for the number of bubbles per event and partons per bubble as a function of percent centrality bins.

In Fig. 1 to Fig. 5 we used the STAR-calculated CI correlation, which displays the average correlation of the unlike-sign charge pairs correlation plus the like-sign charge pairs correlation. To allow comparison with the different centrality bins we and also STAR multiplied by the multiplicity, because, as explained previously, this removes the dilution of the signals owing to the quadratic increase of pair combinations. The multiplicity that is used in Ref. [13] is based on the particles measured in the STAR TPC. There are readout boundaries between the 12 TPC sectors that cover the azimuth that do not measure tracks. We put these readout boundaries in our Monte Carlo generation of our particles, which causes a loss of approximately 10% of the particles.

TABLE II. Impact parameters of HIJING with centrality.

Centrality	Impact parameter (fm)
0%–5%	0.0–2.9
5%–10%	2.9–4.1
10%–20%	4.1–5.8
20%–30%	5.8–7.1
30%–40%	7.1–8.2
40%–50%	8.2–9.2
50%–60%	9.2–10.1
60%–70%	10.1–10.9
70%–80%	10.9–11.7

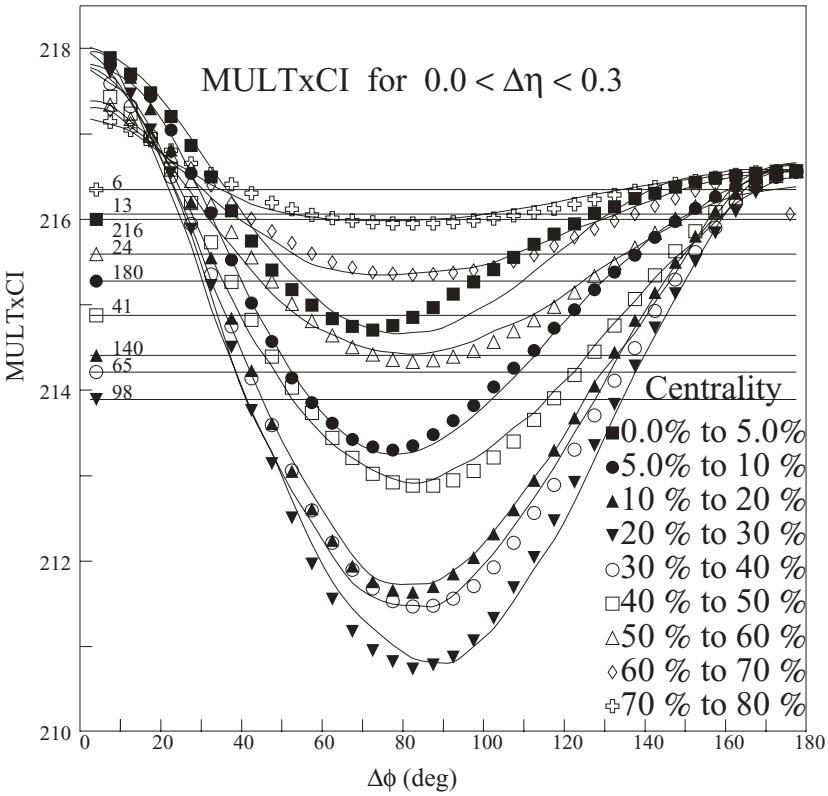

FIG. 1. The multiplicity (MULT) times the CI correlation vs $\Delta\phi$ for $0.0 < \Delta\eta < 0.3$. Nine centralities are shown from 0% to 80% with centrality bins increasing from 0% to 5%. The multiplicity for 0% to 5% is 216; all other centralities are shifted upward so that their 180° values are equal. Each multiplicity for each centrality is shown shifted. The solid curves are the bubble model (PMBE) calculations shifted by the same amount as the data. The PBME and RHIC data agree within a few percent of the total CI correlation in each centrality bin in each $\Delta\eta$ range for all $\Delta\phi$ angles.

The multiplicity-scaled correlation for each centrality for a given $\Delta\eta$ bin is plotted with the maximum angle of the away side ($\Delta\phi = 180°$) shifted to the same value. The horizontal line for each centrality shows the shifted average multiplicity line, which was normalized to a mean of 1 in the original CI correlation and became equal to the average multiplicity after becoming rescaled to the scaled correlation. The solid curves are the PBME calculations shifted by the same amount as the data. The agreement between the PBME and the RHIC data in Figs. 1 to 5 is within a few percent of the total correlation.

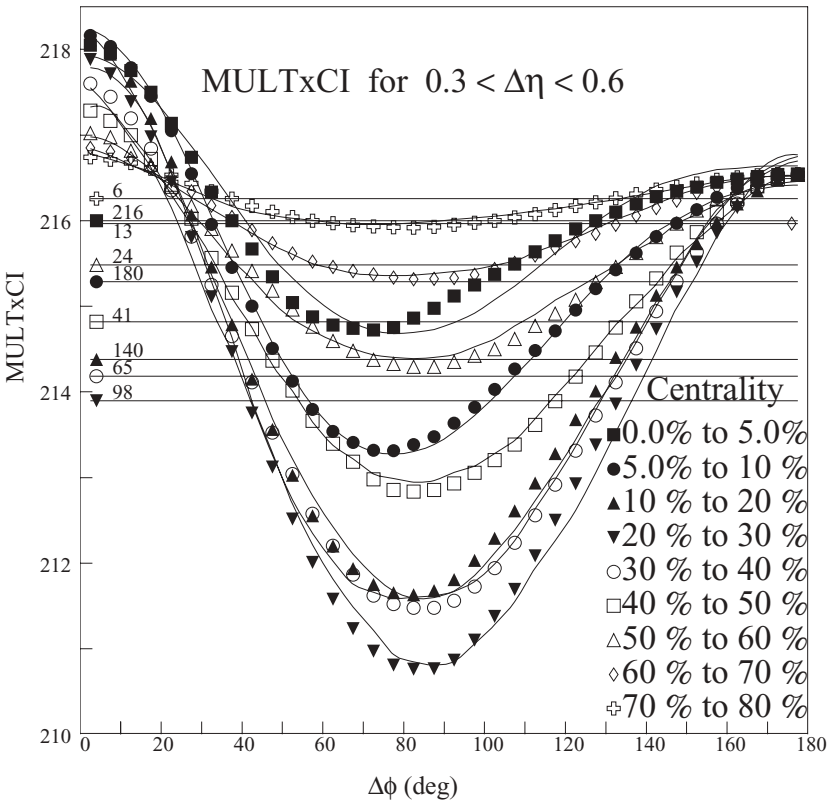

FIG. 2. The multiplicity (MULT) times the CI correlation vs $\Delta\phi$ for $0.3 < \Delta\eta < 0.6$. Nine centralities are shown from 0% to 80% with centrality bins increasing from 0% to 5%. The multiplicity for 0% to 5% is 216; all other centralities are shifted upward so that their 180° values are equal. Each multiplicity for each centrality is shown shifted. The solid curves are the bubble model (PBME) calculations shifted by the same amount as the data. The PBME and the RHIC data agree within a few percent for the total CI correlation.

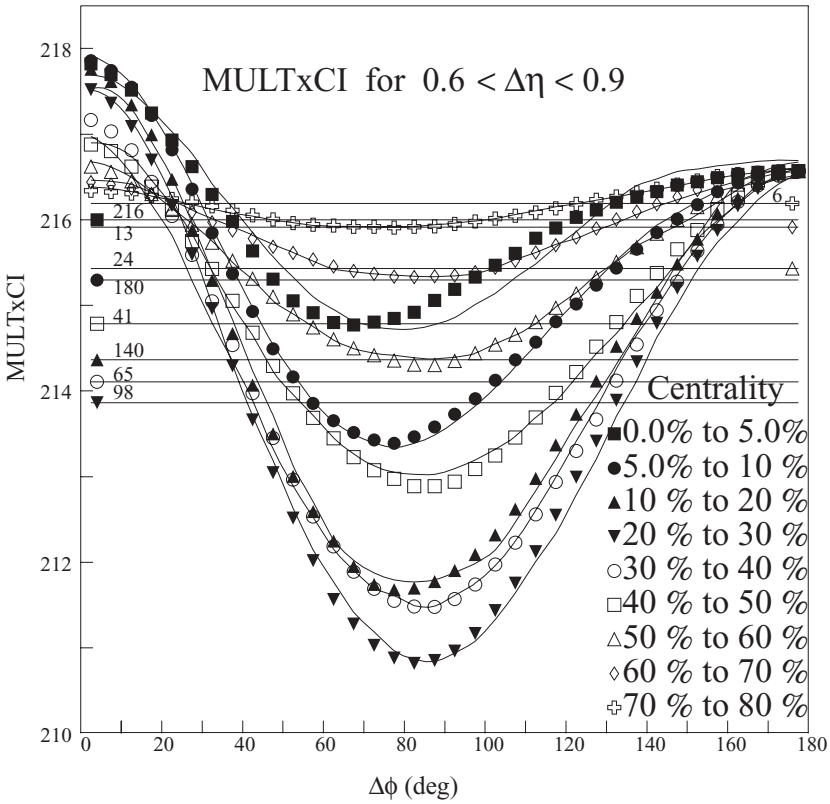

FIG. 3. The multiplicity (MULT) times the CI correlation vs $\Delta\phi$ for $0.6 < \Delta\eta < 0.9$. Nine centralities are shown from 0% to 80% with centrality bins increasing from 0% to 5%. The multiplicity for 0% to 5% is 216; all other centralities are shifted upward so that their 180° values are equal. Each multiplicity for each centrality is shown shifted. The solid curves are the bubble model (PBME) calculations shifted by the same amount as the data. The PBME and the RHIC data agree within a few percent for the total CI correlation.

Considering that the model (PBME) does not completely include important nonperturbative QCD effects contained in the data we consider this a reasonable quantitative agreement. The CI times multiplicity displays the average structure of the correlation sources at kinetic freezeout.

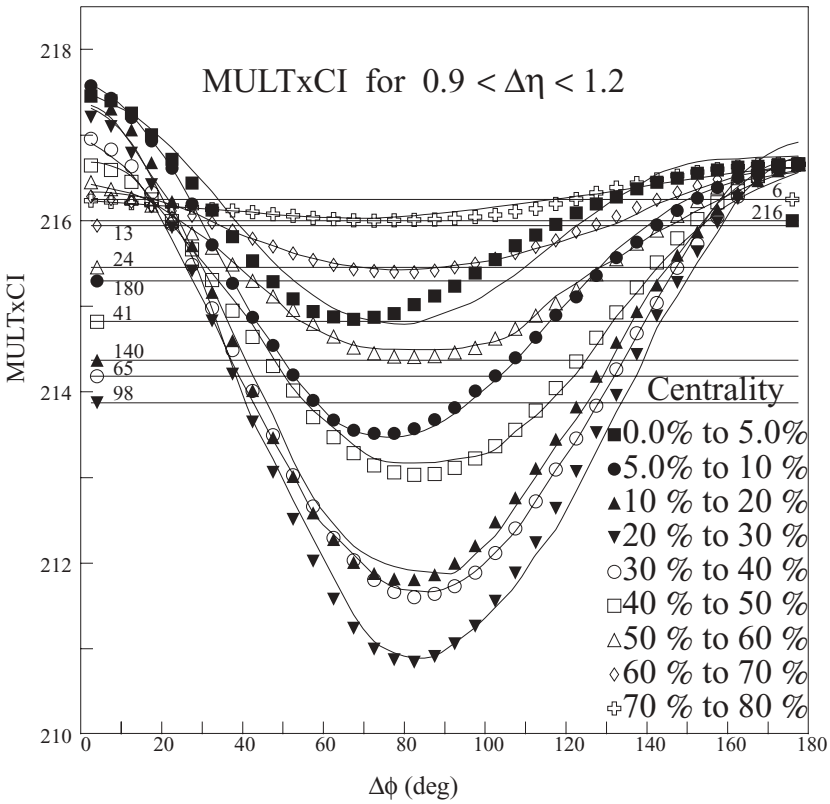

FIG. 4. The multiplicity (MULT) times the CI correlation vs $\Delta\phi$ for $0.9 < \Delta\eta < 1.2$. Nine centralities are shown from 0% to 80% with centrality bins increasing from 0% to 5%. The multiplicity for 0% to 5% is 216; all other centralities are shifted upward so that their 180° values are equal. Each multiplicity for each centrality is shown shifted. The solid curves are the bubble model (PBME) calculations shifted by the same amount as the data. The PBME and the RHIC data agree within a few percent for the total CI correlation.

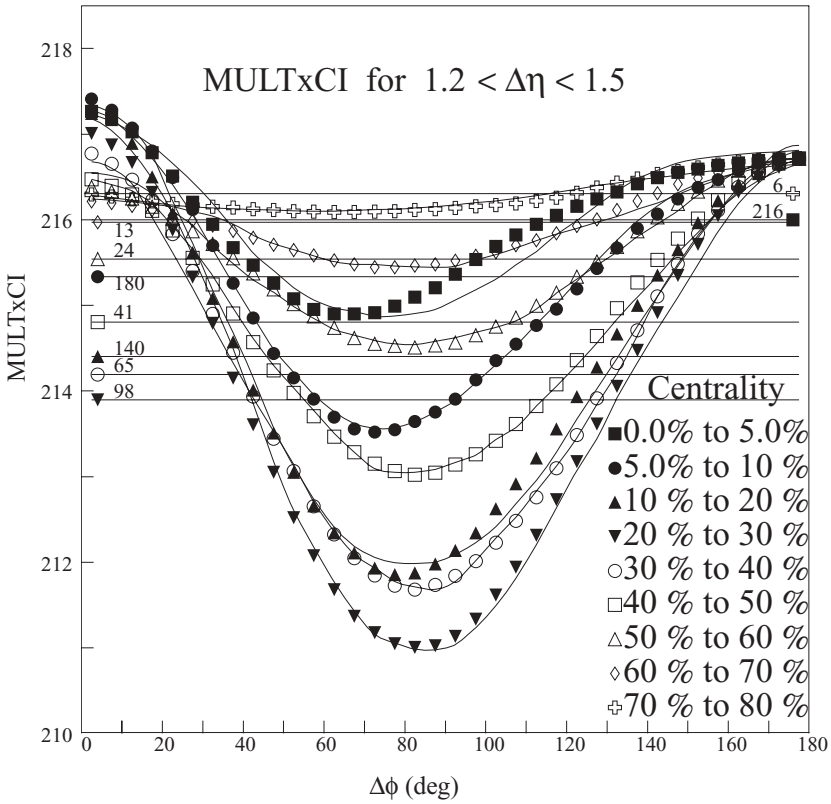

FIG. 5. The multiplicity (MULT) times the CI correlation vs $\Delta\phi$ for $1.2 < \Delta\eta < 1.5$. Nine centralities are shown from 0% to 80% with centrality bins increasing from 0% to 5%. The multiplicity for 0% to 5% is 216; and all other centralities are shifted upward so that their 180° values are equal. Each multiplicity for each centrality is shown shifted. The solid curves are the bubble model (PBME) calculations shifted by the same amount as the data. The PBME and the RHIC data agree within a few percent for the total CI correlation.

VI. CHARGE-DEPENDENT CORRELATION

We compare total experimentally observed CD correlations to total theoretically predicted CD correlations to avoid possible uncertainties owing to separation of signals and background.

The CD correlation, which is the difference between the unlike-sign charge pairs correlations and the like-sign

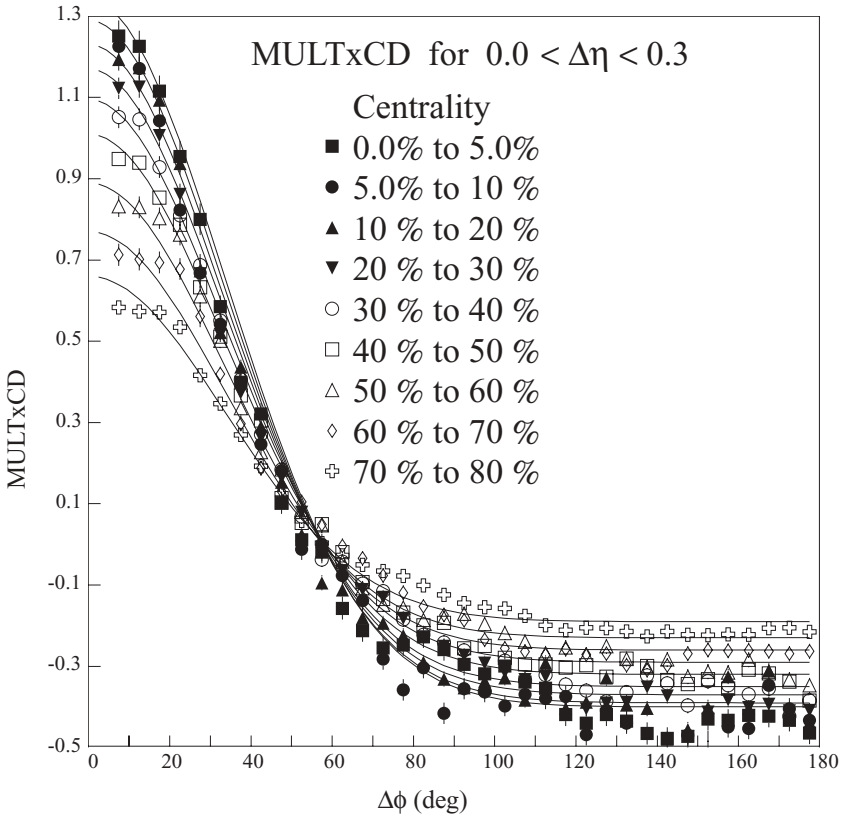

FIG. 6. The multiplicity (MULT) times the CD correlation vs $\Delta\phi$ for $0.0 < \Delta\eta < 0.3$. Nine centralities are shown from 0% to 80% with centrality bins increasing from 0% to 5%. The solid curves are the bubble model (PBME) calculations scaled by the multiplicity. We get good agreement.

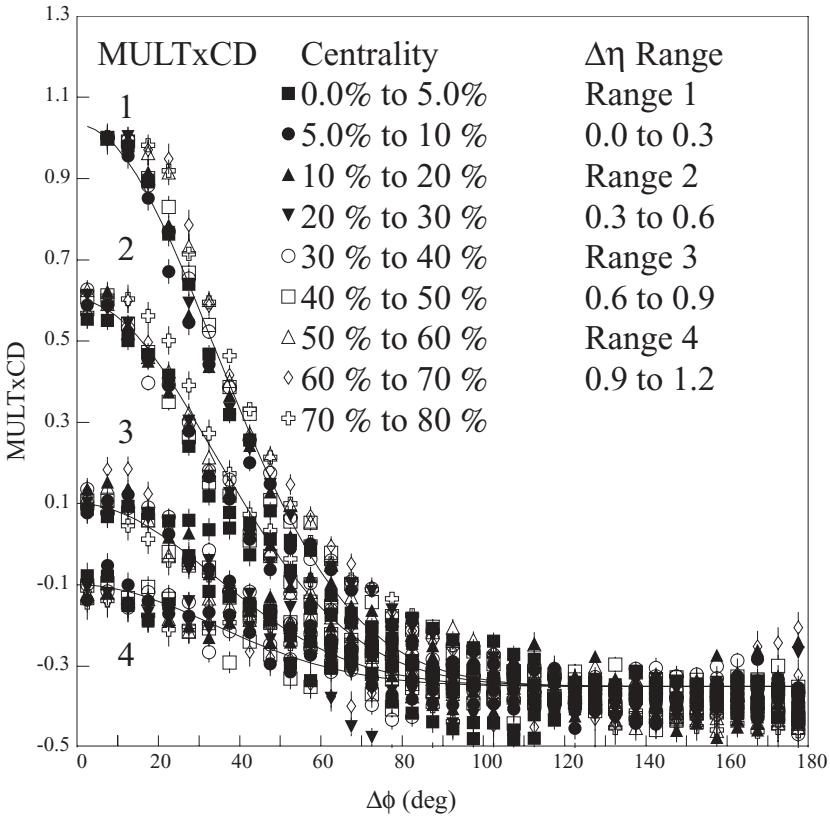

FIG. 7. The product of the multiplicity (MULT) and the CD correlation vs $\Delta\phi$ for four $\Delta\eta$ bins. Nine centralities are shown from 0% to 80% with centrality bins increasing from 0% to 5%. Each of the centralities is scaled so that the 5°–10° $\Delta\phi$ bin for the $\Delta\eta$ range 0.0 to 0.3 is normalized to 1. The data points for each $\Delta\eta$ range cluster around the PYTHIA jet predictions (lines). Thus we see that the CD shape is approximately independent of centrality and the CD is approximately consistent with PYTHIA jets [20] (line) at each centrality. The PBME fits the observed CD correlation to within a few percent of the correlation at all centralities since its predicted shape is given by PYTHIA jets and we get a good agreement for multiplicity-scaled CD correlation for each of the centralities.

charge pairs correlations (US − LS) displays a measure of the emission correlation of the opposite sign pairs of particles emitted from the same space-time region at the time of hadronization [10,23]. The CD in the PBME (which includes a HIJING jet component) has its fragmentation of all partons, in all centralities, determined by PYTHIA fragmentation [20]. We use the same projection method of the 2-D CD correlation into the same five $\Delta\eta$ ranges and multiply the CD by the multiplicity, as described and discussed in Sec. V. In Fig. 6 we show the multiplicity times the CD $\Delta\phi$ correlation from Ref. [13] within the $\Delta\eta$ range 0.0 to 0.3 for each centrality compared to the bubble model (PBME) calculations. We achieve a good agreement between data and model. Similar results and good agreement with the PBME occurs for the four other $\Delta\eta$ ranges not shown. Thus we have good agreement in all five $\Delta\eta$ ranges, which together comprise the entire CD.

In Fig. 7 we plot from Ref. [13] the CD $\Delta\phi$ correlation for four $\Delta\eta$ bins covering the range $0.0 < \Delta\eta < 1.2$.[1] Each of nine centralities shown were scaled so that the 5°–10° $\Delta\phi$ bin for the $0.0 < \Delta\eta < 0.3$ range is normalized to 1. This was done to remove the scale difference between the different centrality ranges and allow us to show that the CD shape is approximately independent of centrality. In Fig. 7 the experimental analysis points in each $\Delta\eta$ range cluster around the four lines that correspond to each of the four $\Delta\eta$ ranges generated by PYTHIA jets [20]. PYTHIA jets were used as the jets in HIJING, and PYTHIA fragmentation was used in the parton bubble model [8]. Thus the CD shape is in good agreement with PYTHIA and is independent of centrality. PYTHIA jet CD correlations are the initial correlations of opposite-sign charge pairs from the same space-time region at the time of hadronization [10,23]. The fact that there is essentially no change in these correlations at the time of kinetic freezeout demonstrates that there is little or no further interaction of these opposite-sign charge pairs with the fireball medium from the time of hadronization till the time of kinetic freezeout. Thus both hadronization and kinetic freezeout occur at or very near the surface of the expanding fireball at all centralities. Hence in general the fireball is dense and opaque at kinetic freezeout. One should note that in the peripheral bins there is very little matter in the short path length from any point to the surface. This is consistent with surface emission from the fireball at kinetic freezeout or undisturbed fragmentation in those peripheral bins where the path length to the surface is small.

Both the original parton bubble model (PBM) [8] and the present extension of the model (PBME) construct surface bubbles that are boosted by the expanding fireball. These bubbles at freezeout give results that are consistent with experimental correlation data [13]. Furthermore, the PBME fits the observed CD correlation to within a few percent of the correlation at all centralities. The PBME produces the CD shape that is consistent with PYTHIA jet CD correlations. As previously shown in Sec. V the PBME fits the observed CI correlations to within a few percent of the correlation. The US and LS correlations are linear combinations of the CI and

[1]The $\Delta\eta$ range of 1.2 to 1.5 (not shown) is just a flat background with very little CD signal from PYTHIA parton fragmentation left.

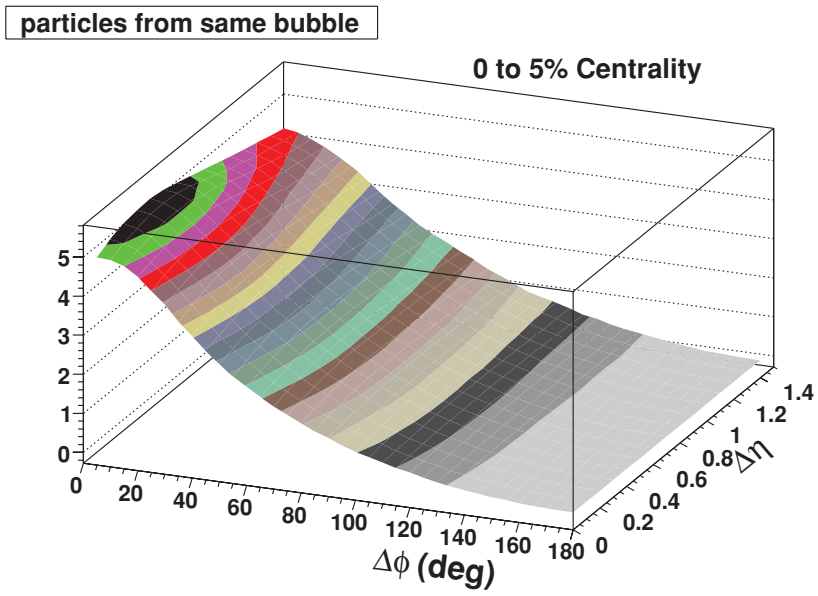

FIG. 8. (Color online) The multiplicity (MULT) times the CI correlation for the 0%–5% centrality bin as a 2-D $\Delta\phi$ vs $\Delta\eta$ perspective plot. This is the part of the CI correlation that resulted from particles emitted from the same bubble.

CD. Therefore they are also fit to within a few percent of the correlation. Thus all two-charge-particle-pair correlations are reasonably quantitatively fit by the PBME. One should note that the fireball in both the PBM and PBME is treated in a blast wave model with the bubbles forming on the surface and emitting their final-state particles at kinetic freezeout. The fireball surface is moving at the maximum velocity at kinetic freezeout.

VII. FURTHER DISCUSSION OF THE PARTON BUBBLE MODEL CORRELATION

We note from Tables I–III that as we move from the most central region (small impact parameter) toward the peripheral bins the number of bubbles in a centrality bin per event and the number of partons per bubble both tend to decrease. In the two most peripheral bins bubble production is negligible.

Figures 8 and 9 are 2-D perspective plots (in $\Delta\phi$-$\Delta\eta$ space) of the part of the CI correlation multiplied by the multiplicity (multiplicity scaled) that results from particles emitted from the same bubble in the centrality bins shown. The $\Delta\phi$ angular distributions of the correlation are primarily confined to the near side ($\Delta\phi < 90^\circ$). The shape of the $\Delta\phi$ correlation for 0%–30% centrality bins peak near small angles and decrease as $\Delta\phi$ increases toward 90° and are qualitatively similar. However, the $\Delta\eta$ distribution shape remains qualitatively broad in the 0%–30% centrality bins, exhibiting the $\Delta\eta$ elongation observed in the data [13]. One should note that there is very little away-side ($\Delta\phi > 90^\circ$) contribution in any of these centrality bins.

TABLE III. Parameters of bubble model per number of partons.

No. partons	Particles per bubble	p_t per bubble (GeV/c)	Energy per bubble (GeV)
3–4	8.5	7.0	9.8
3	7.0	5.7	8.0
2	4.9	4.0	4.9
1	2.6	2.1	2.1

Figure 10 shows a comparison of the bubble signal (particle from the same bubble) shape in $\Delta\eta$ of the different centralities in which we have bubbles. The bubbles with the same number of partons are consistent with the same shape in $\Delta\eta$. Thus the longitudinal (i.e., $\Delta\eta$ distribution) determines the number of partons in each bubble, which determines the longitudinal shape of the bubbles. We can see that there is a maximum expansion in the length of $\Delta\eta$ in the most central bin (0%–5%) and close to this maximum is maintained through the 20%–30% bin. However, the length of $\Delta\eta$ considerably decreases in the 30%–60% bins.

In Ref. [8] the ring of bubbles played an important role in the away-side ($\Delta\phi 180^\circ$) correlation. Correlation between particles from different bubbles show an away-side correlation. Figures 11 and 12 show the correlation that resulted from all particles from all the bubbles. We plot this correlation for all centralities where there are bubbles present.

If we compare Fig. 8 and Fig. 9 (multiplicity-scaled CI for particles from the same bubble) with Fig. 11 and Fig. 12 (multiplicity-scaled CI for particles from all bubbles) we note a striking difference in the away-side ($\Delta\phi > 90^\circ$) behavior of the two sets. The correlation resulting from particles emitted by the same bubble produces an away side that is very small (Fig. 8 and Fig. 9). The away-side correlation produced by particles emitted by all bubbles is large in the centrality range 0%–30%, where bubble production is large, and then essentially disappears for the more peripheral centralities, where the bubble production becomes small to negligible (Fig. 11 and Fig. 12). This is due to the model conserving momentum between the bubbles and is consistent with the experimental observations.

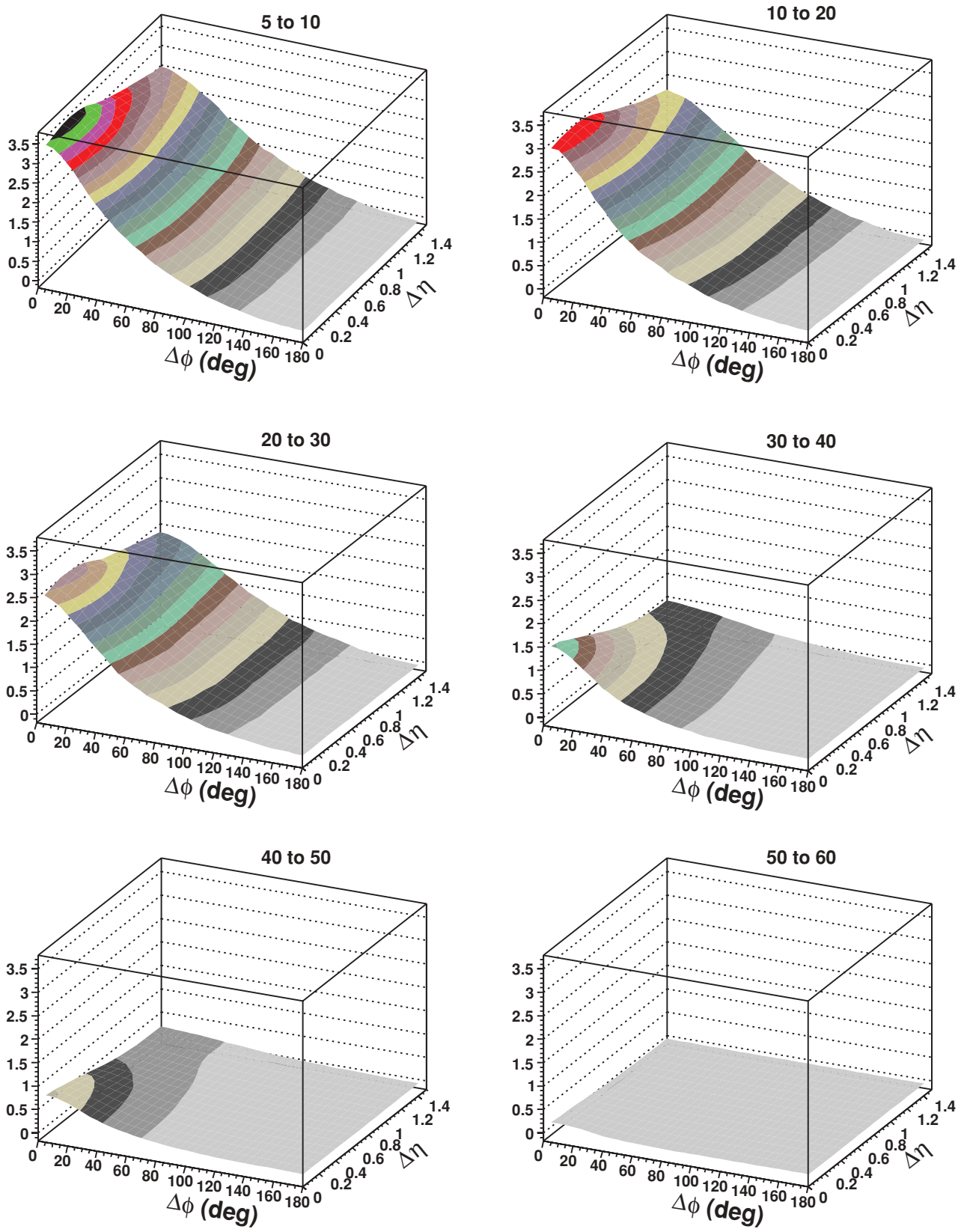

FIG. 9. (Color online) The multiplicity (MULT) times the CI correlation for the six centralities as six 2-D $\Delta\phi$ vs $\Delta\eta$ perspective plots. This is the part of the CI correlation that resulted from particles emitted from the same bubble. We see in Fig. 8 and Fig. 9 that the multiplicity-scaled correlation grows with centrality. The correlation for $\Delta\eta$ remains large, decreases little in the 0%–30% centrality bins, and decreases sharply beyond that.

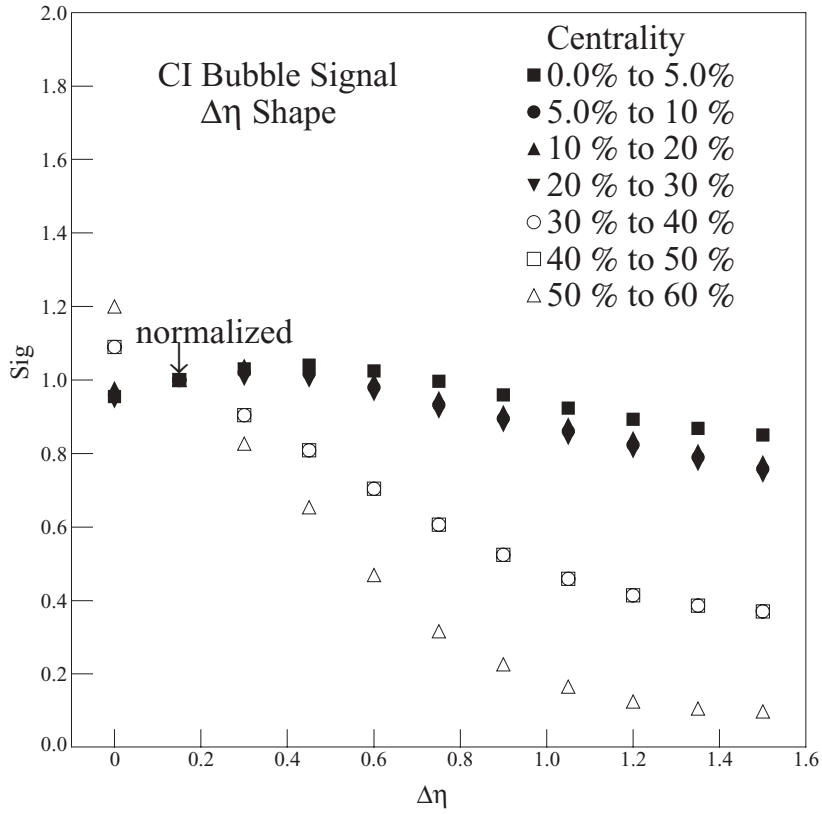

FIG. 10. The CI correlation bubble signal shape normalized to one at $\Delta\eta = 0.15$ vs $\Delta\eta$ for $10^\circ < \Delta\phi < 20^\circ$. Seven centrality bins where there are bubbles present in our model are shown from 0% to 60% with increasing bin size from 5% to 10%. The CI bubble signal $\Delta\eta$ is broad and similar (roughly constant) as a function of $\Delta\eta$ for the 0%–30% centrality range. From the tables and text discussion we find that bubbles in this centrality range contains 3–4 partons each and that it is the number of partons that determine the $\Delta\eta$ width. The 30%–60% centrality range shows that the bubble signal $\Delta\eta$ width decreases as the number of partons decrease from 3 to 1.

Our model results in bubbles forming where energy density is highest. Thus as we have pointed out the most central collisions have the highest energy density, and therefore a circular ring of bubbles perpendicular to and centered on the beam axis was able to explain the correlations observed in a $\sqrt{s_{NN}} = 200$ GeV Au + Au RHIC central production experimental analysis [8,10]. The PBME has explained the new experimental analysis as a function of centrality [13]. However, as we move away from central production bins toward peripheral bins the highest energy density concentrates in the region of the reaction plane, the central ring symmetry is broken, and the bubbles tend to be produced in the reaction plane region. Thus the geometry of the bubbles become coupled to elliptic flow.

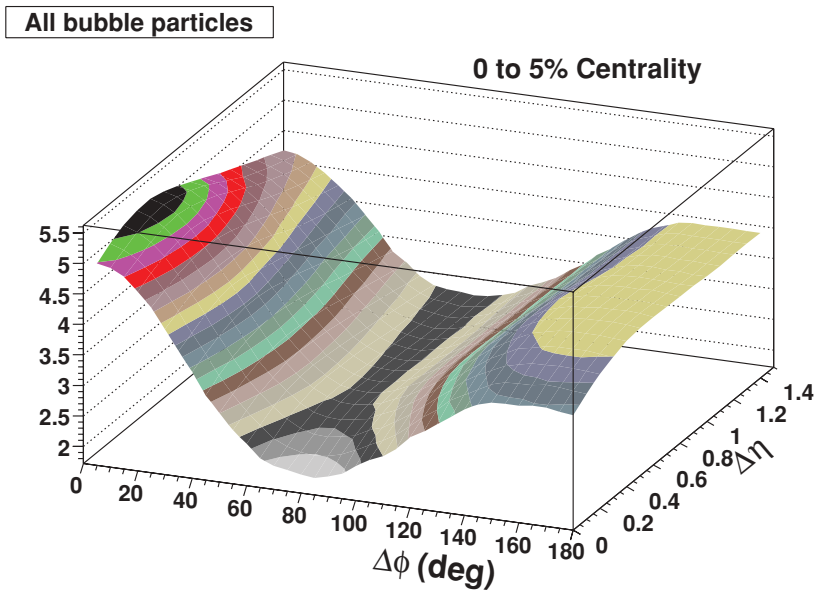

FIG. 11. (Color online) The multiplicity (MULT) times the CI correlation for the 0%–5% centrality bin as a 2-D $\Delta\phi$ vs $\Delta\eta$ perspective plot. This is the part of the CI correlation that resulted from particles emitted from all the bubbles.

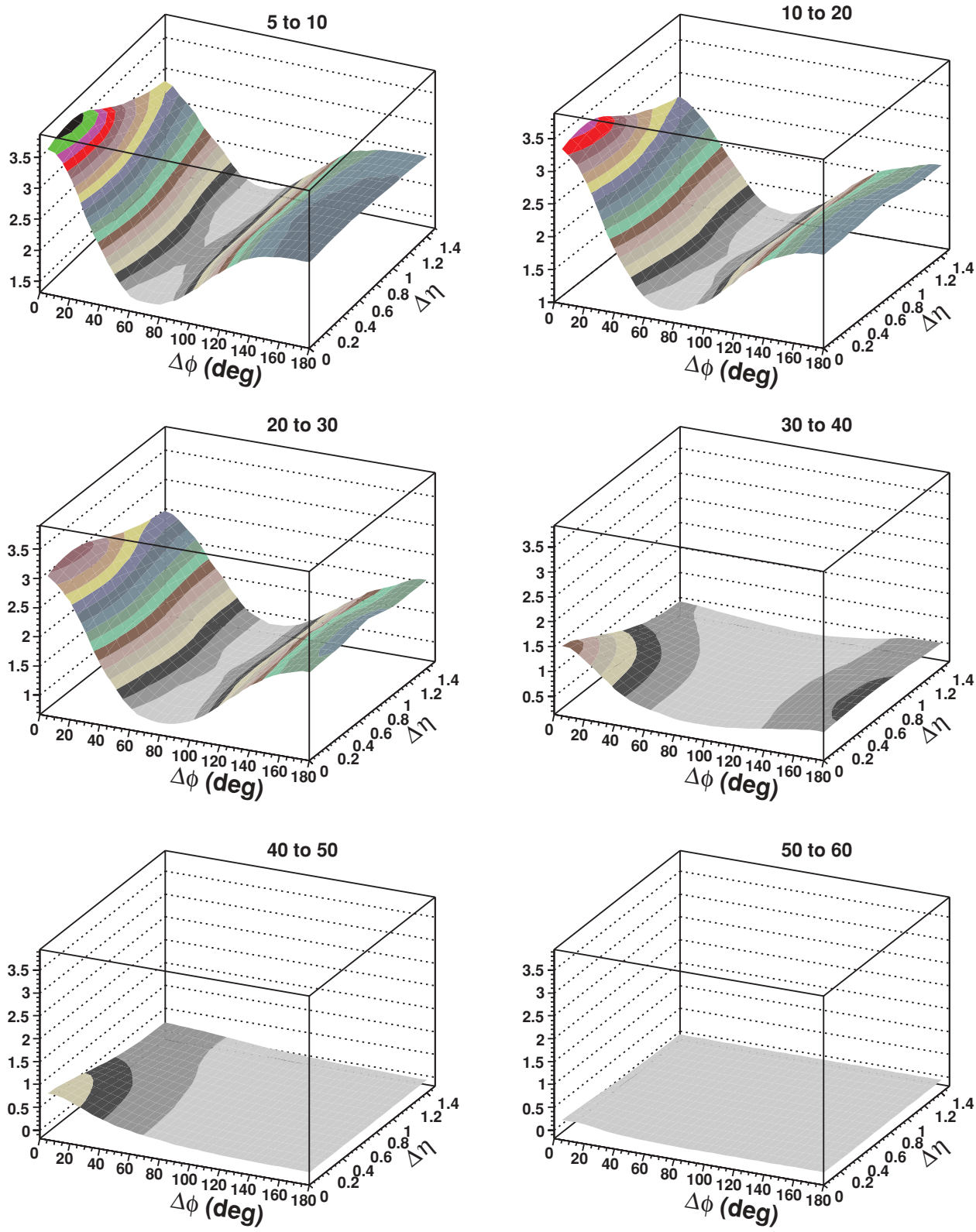

FIG. 12. (Color online) The multiplicity (MULT) times the CI correlation for the six centralities plotted as six 2-D $\Delta\phi$ vs $\Delta\eta$ perspective plots. This is the part of the CI correlation that resulted from particles emitted from all the bubbles. We see that the multiplicity-scaled CI correlation in Fig. 11 and Fig. 12 from all the bubbles behaves similar to that from the CI part, which results from a single bubble as shown in Fig. 8 and Fig. 9 with one important striking difference. There is a large away-side (>90°) correlation in the 0%–30% centrality range where there is large bubble production. This is due to the model conserving momentum between the bubbles and is consistent with the experimental observations.

VIII. SUMMARY AND DISCUSSION

In this article we summarize the assumptions made and the reasoning that led to the development and construction of our parton bubble model [8], which successfully explained the charge particle pair correlations in the central (approximately 0%–10% centrality) $\sqrt{s_{NN}} = 200$ GeV Au + Au data [10]. The PBM was also consistent with the central collision Au + Au HBT results. This is presented and discussed in Sec. 4 of Ref. [8] and Sec. II of this paper. Most of this paper is concerned with extending our model, which was a central region model, to be able to treat the geometry of bubble production for 0%–80% collision centralities (PBME) such as measured and analyzed in recent RHIC data [13]. In the PBME we included elliptic flow for all centralities and a jet component for centralities of 30%–80%, both of which become large while bubble production becomes smaller as the centrality becomes more peripheral. We were able to extend the PBM to the PBME and reasonably fit the new quantitative RHIC 0%–80% $\sqrt{s_{NN}} = 200$Au + Au data [13] for the CI and CD correlations. We demonstrated that the PBME had a bubble geometry that tracked the highest energy density of the different centralities. The most central collisions have a symmetry about the beam axis. The region of highest energy density will also be symmetric about this axis and the ring of bubbles centered on this axis is the expected geometry, being nearly identical to that of the PBM.

As we move to more peripheral collisions the energy density decreases. The symmetry of highest energy density becomes coupled to elliptic flow and is defined by the reaction plane. The region of highest energy density becomes concentrated in the reaction plane region. Therefore the ring symmetry that applies to central production was broken and the bubbles farthest from the reaction plane disappear. The 12 bubbles for the most central bin (0%–5%) reduce to 10 (5%–10%), then to 7 (10%–20%), and then to 5 bubbles (20%–30%). Moving to 30%–40%, 40%–50%, and 50%–60% we find that the bubbles are in the reaction plane region with the probability per event of making a bubble being 1.5, 0.6, and 0.3, respectively (see Table I).

Both the PBM and the PBME treat the fireball in a blast wave model. Bubbles are formed on the surface of the blast wave fireball, which emits the final-state particles at kinetic freezeout. We achieve reasonable fits to the quantitative STAR experimental analysis of the charge-independent and the charge-dependent correlations within a few percent of the total correlations [13]. These correlations considered particles in the p_t range from 0.8 to 4.0 GeV/c. The model is also consistent with the HBT results in this p_t range. The CI correlation displays the average structure of the correlated emitting sources at kinetic freezeout. The CD correlation has the initial emission correlation of the opposite-sign charge pairs of particles emitted from the same space-time region at the time of hadronization. This initial correlation should remain consistent with the CD correlation of PYTHIA jets if there are no further interactions with other particles after hadronization. The analysis demonstrated that at kinetic freezeout the CD correlation in this p_t range was consistent with PYTHIA jets at all centralities (see Sec. VI). Therefore one concludes that hadronization and kinetic freezeout both occur at or very near the surface of the fireball at all centralities. Thus the expanding fireball is dense and opaque for most centralities at kinetic freezeout. Of course the most peripheral bins, owing to the low material content, allow small path length to the surface. Both the PBM and its extended present version PBME are surface-emission models and thus are consistent with this striking experimental feature.

It is of interest to note that the parton bubble model central collision analysis [8] has recently been pointed out in Ref. [24] as having features in common with glasma flux tubes, which evolve from initial color glass condensates. This supports the hypothesis that the bubble substructure can be considered a QGP signal and may serve as a key in investigating both QGP and glasma effects.

The persistence of the production of similar surface bubbles at kinetic freezeout in numbers that decrease as the highest energy density decreases as the centrality is decreased (going toward the peripheral bins) and their general characteristic of being produced in the region of highest energy density implies the following:

(i) The bubbles represent a significant substructure of gluonic hot spots formed on the surface of a dense opaque fireball at kinetic freezeout. The number of bubbles formed and the energy content of each of these substructures is a function of the energy density and its extent in space.

(ii) Their characteristics, persistence, and behavior as a function of centrality and the PBME reasonably quantitative fits to the CI and CD data at all centralities provide substantial evidence that the bubbles are the final-state products of QGP production. If sufficiently convincing QGP signatures can be extracted from these bubbles then one could eventually provide substantial evidence for a QGP. We will be investigating this in future work. The bubbles may contain relevant information on other topics of interest (e.g., glasma), which we will also investigate. In our future program we plan to utilize the anticipated forthcoming availability of time-of-flight particle identification data at STAR to further study charged particles correlations with identified particles. In the second paragraph from the end of Sec. 1.2 of Ref. [8] we speculated on the possibility of applying these model ideas (suitably modified) to LHC data when they become available.

ACKNOWLEDGMENTS

The authors thank William Love for valuable discussion and assistance in production of figures. This research was supported by the U.S. Department of Energy under Contract No. DE-AC02-98CH10886 and the City College of New York Physics Department of the City University of New York.

[1] L. van Hove, Z. Phys. C **27**, 135 (1985).
[2] J. A. Lopez, J. C. Parikh, and P. J. Siemens, Phys. Rev. Lett. **53**, 1216 (1984).
[3] S. Pratt, P. J. Siemens, and A. P Vischer, Phys. Rev. Lett. **68**, 1109 (1992).
[4] M. Gyulassy, D. Rischke, and B. Zhang, Nucl. Phys. **A613**, 397 (1997).
[5] A. Dumitru and D. Pisarski, Phys. Lett. **B504**, 282 (2001).
[6] H. J. Drescher, F. M. Liu, S. Ostapchenko, T. Pierog, and K. Werner, Phys. Rev. C **65**, 054902 (2002).
[7] S. J. Lindenbaum and R. S. Longacre, J. Phys. G **26**, 937 (2000).
[8] S. J. Lindenbaum and R. S. Longacre, Eur. Phys. J. C **49**, 767 (2007).
[9] J. Adams *et al*., Phys. Rev. C **71**, 044906 (2005); S. S. Adler *et al*., Phys. Rev. Lett. **93**, 152302 (2004).
[10] J. Adams *et al*., Phys. Rev. C **75**, 034901 (2007).
[11] J. Adams *et al*., Phys. Rev. C **70**, 054907 (2004).
[12] F. Karsch, Nucl. Phys. **A698**, 199c (2002).
[13] B. I. Abelev *et al*., arXiv:0806.0513 [nucl-ex]; R. S. Longacre, Quark Matter 2006, nucl-ex/0702008.
[14] S. J. Lindenbaum, R. S. Longacre, and M. Kramer, Eur. Phys. J. C **30**, 241 (2003).
[15] K. Kajantie, P. V. Landshoff, and J. Lindfors, Phys. Rev. Lett. **59**, 2527 (1987).
[16] C. Adler *et al*., Phys. Rev. Lett. **88**, 022301 (2002).
[17] J. Adams *et al*., Phys. Rev. Lett. **91**, 172302 (2003).
[18] A. Adare *et al*., arXiv:0801.4020 [nucl-ex] (submitted to Phys. Rev. Lett).
[19] X. N. Wang and M. Gyulassy, Phys. Rev. D **44**, 3501 (1991).
[20] T. Sjostrand and M. van Zijl, Phys. Rev. D **36**, 2019 (1987).
[21] B. Andersson, J. Gustafson, G. Ingelman, and T. Sjostrand, Phys. Rep. **97**, 31 (1983).
[22] J. Adams *et al*., Phys. Rev. C **72**, 014904 (2005).
[23] S. A. Bass, P. Danielewicz, and S. Pratt, Phys. Rev. Lett. **85**, 2689 (2000); S. Cheng *et al*., Phys. Rev. C **69**, 054906 (2004); P. Christakoglou, A. Petridis, and M. Vassiliou, Nucl. Phys. **A749**, 279c (2005).
[24] A. Dumitru, F. Gelis, L. McLerran, and R. Venugopalan, Nucl. Phys. **A810**, 91 (2008).